ChemPubSoc Europe

DOI: 10.1002/chem.201701389

CHEMISTRY A European Journal Communication

Carbon Nanotubes

MOF-Templated Assembly Approach for Fe_3C Nanoparticles Encapsulated in Bamboo-Like N-Doped CNTs: Highly Efficient Oxygen Reduction under Acidic and Basic Conditions

Arshad Aijaz,[a] Justus Masa,[c] Christoph Rösler,[d] Hendrik Antoni,[a] Roland A. Fischer,[e, f] Wolfgang Schuhmann,*[c] and Martin Muhler*[a, b]

Abstract: Developing high-performance non-precious metal catalysts (NPMCs) for the oxygen-reduction reaction (ORR) is of critical importance for sustainable energy conversion. We report a novel NPMC consisting of iron carbide (Fe_3C) nanoparticles encapsulated in N-doped bamboo-like carbon nanotubes (b-NCNTs), synthesized by a new metal-organic framework (MOF)-templated assembly approach. The electrocatalyst exhibits excellent ORR activity in 0.1 M KOH (0.89 V at -1 mA cm^{-2}) and in 0.5 M H_2SO_4 (0.73 V at -1 mA cm^{-2}) with a hydrogen peroxide yield of below 1% in both electrolytes. Due to encapsulation of the Fe_3C nanoparticles inside porous b-NCNTs, the reported NPMC retains its high ORR activity after around 70 hours in both alkaline and acidic media.

The oxygen-reduction reaction (ORR) is a key process in fuel cells and metal-air batteries.[1] The current state-of-the-art catalysts for this sluggish cathodic reaction are based on platinum and its alloys.[2] However, the limited availability, high cost, and insufficient durability of platinum preclude its long-term wide-scale use. In recent years, non-precious metal catalysts (NPMCs), especially metal-nitrogen-carbon (M-N-C, M = Co, Fe, or Mn), have drawn much attention owing to their low cost and high catalytic ORR activity.[3,4] NPMCs are very promising catalysts under harsh ORR conditions, but need further improvement in terms of synthetic approach and durability. Very few NPMCs have been found to have sufficient ORR activity and stability in the more challenging acidic media.[5,6] Therefore, platinum is still the most-used ORR catalyst.

The use of metal–organic frameworks (MOFs) as self-sacrificial templates for porous carbon was first reported in 2008 by Xu et al.,[7d] resulting in an enormous upsurge of interest in MOF-derived nanostructured materials for energy storage and conversion applications.[7] MOF-derived NPMCs often exhibit large surface area and hierarchical porous structures, which are essential for high ORR performance.[8] Recently, NPMCs based on iron carbide (Fe_3C) encapsulated in carbon nanostructures have been reported to be very active towards the ORR.[3,5] For example, Yu and co-workers synthesized Fe_3C nanoparticles encapsulated in porous Fe–N-doped carbon fibers exhibiting high ORR activity.[5a] Jia and Guo et al. found that bamboo-like carbon nanotube (CNT)/Fe_3C composites had excellent ORR activity in both alkaline and acidic media.[5b] Li and co-workers demonstrated very efficient ORR electrocatalysis using hollow spheres of Fe_3C nanoparticles encased in graphitic layers.[5c] Encapsulating metal nanoparticles inside carbon structures provides a unique synergistic effect, which also activates the adjacent atoms surrounding the nanoparticle, and the outer surface carbon atoms for the ORR.[9] In addition, encapsulation provides resistance against corrosion of the metal nanoparticles, especially in acidic electrolytes, which is a necessary prerequisite to ensure long-term performance.[10] Very few studies have reported the synthesis of Fe_3C-based catalysts from MOF precursors, probably because of two reasons. Firstly, carbonization of the Fe-MOF mostly leads to a mixed-phase product such as Fe_3C, iron oxide, or metallic iron;[11] this complicates unambiguous identification of the true active sites for the ORR. Secondly, the prepared catalysts do not have well-defined nanostructures.[12] Hence, new synthesis strategies are needed to explore the potential of MOF-derived nanostructured Fe-electrocatalysts. Herein, we report a new MOF-template-assembly strategy for the synthesis of a new NPMC consisting of Fe_3C nanoparticles encapsulated in porous bamboo-like N-doped carbon nanotubes. The as-synthesized catalyst possess-

[a] Dr. A. Aijaz, H. Antoni, Prof. Dr. M. Muhler
Laboratory of Industrial Chemistry
Ruhr-University Bochum, 44780 Bochum (Germany)
E-mail: muhler@techem.rub.de

[b] Prof. Dr. M. Muhler
Max Planck Institute for Chemical Energy Conversion
45470 Mülheim an der Ruhr (Germany)

[c] Dr. J. Masa, Prof. Dr. W. Schuhmann
Analytical Chemistry–Center for Electrochemical Sciences (CES)
Ruhr-University Bochum, 44780 Bochum (Germany)
E-mail: wolfgang.schuhmann@rub.de

[d] C. Rösler
Anorganische Chemie II, Organometallics & Materials
Ruhr-University Bochum, 44780 Bochum (Germany)

[e] Prof. Dr. R. A. Fischer
Department of Chemistry, Technical University Munich
Lichtenbergstrasse 4, 85748 Garching (Germany)

[f] Prof. Dr. R. A. Fischer
Catalysis Research Centre, Technical University Munich
Ernst-Otto-Fischer-Strasse 1, 85748 Garching (Germany)

Supporting Information and the ORCID identification number(s) for the author(s) of this article can be found under https://doi.org/10.1002/chem.201701389.

Part of a Special Issue to celebrate the 150th anniversary of the German Chemical Society (GDCh). To view the complete issue, visit https://doi.org/chem.v23.50.

es the desired features for efficient ORR, including intrinsic active sites (in the forms of Fe_3C@carbon, Fe–N_x/C, or N-doped carbon), high surface area, and nanoporous structure; as well as a highly graphitic bamboo-like carbon framework. As a result, the electrocatalyst showed excellent ORR activity and stability in both alkaline and acidic media.

In a typical synthesis, 1.0 g of ZIF-8 (preactivated at 200 °C under vacuum), and 1.0 g of pyrrole were thoroughly mixed, followed by dropwise addition of an aqueous solution of $FeCl_3{\cdot}6H_2O$ (6.0 mL, 0.1 M) over a period of roughly 3 hours. This led to polymerization of the pyrrole residing inside and outside of the ZIF-8 pores, and coordination of the pyrrole nitrogen atom to Fe^{3+}. ZIF-8 was deliberately chosen because this N-containing Zn-MOF is known for its high thermal and chemical stability, as well as its large surface area with a 1.2 nm cavity size. The resulting homogeneous mixture was left to dry overnight at room temperature. The obtained powder was pyrolyzed at a rate of 5 °C min^{-1} to 800 °C in an N_2 atmosphere, and kept at this temperature for 2 hours. The resulting catalyst is denoted as Fe_3C/b-NCNT, in which b-NCNT refers to bamboo-like nitrogen-doped carbon nanotube.

The powder X-ray diffraction (PXRD) pattern of Fe_3C/b-NCNT displayed a strong peak around 26.5° assigned to the (002) reflection of graphitic carbon, in agreement with the structure of multi-walled CNTs (Figure 1a). The other peaks in Figure 1a located at 37.8, 43.1, 43.1, 43.9, 44.9, 46.0, 48.7, and 49.3° correspond to the Fe_3C phase. No diffraction pattern corresponding to zinc was observed, due to the formation of amorphous zinc metal followed by its vaporization,[8g] although residual 2.8 wt% zinc was found by inductively coupled plasma mass spectrometry (ICP-MS) analysis. Scanning electron microscopy (SEM) and transmission electron microscopy (TEM) analysis of Fe_3C/b-NCNT revealed typical features of b-NCNTs with a diameter of 50–100 nm (Figures 1b, 1c, S1, and S2). Small Fe_3C nanoparticles, visible as black dots in Figure 1c, were distributed mainly within b-NCNTs. High-angle annular dark-field scanning TEM (HAADF-STEM) further identified the encapsulated black particles in b-NCNTs as iron carbide with a lattice distance of 0.21 nm, corresponding to the (211) crystal planes of Fe_3C (Figure 1d). Selected area electron diffraction (SAED) patterns also demonstrated the presence of crystalline Fe_3C (Figure S3). Careful evaluation of the HAADF-STEM images revealed the porous and hollow nature of the b-NCNTs (Figure 1e). We further investigated the elemental distribution in Fe_3C/b-NCNT using HAADF-STEM and energy-dispersive X-ray spectroscopy (EDS) techniques, which indicated the presence of C, N, and Fe (Figures 1f–h). Notably, except for the nanoparticle regions, all elements were homogeneously distributed in the Fe_3C/b-NCNT sample. High uniformity of the Fe species in the b-NCNT matrix was observed at the atomic level, and the Fe and N intensities coincided with each other to a significant degree, suggesting that there are probably Fe species stabilized by N-coordination (so-called Fe–N_x sites), which are commonly assumed to be active sites for the ORR.[5a] In the nanoparticle region, the strong Fe signals and weak C signals were observed simultaneously, which possibly indicates the iron carbide phase. Indeed, PXRD measurement confirmed that the nanoparticles in Fe_3C/b-NCNT are pure Fe_3C.

The porous nature of Fe_3C/b-NCNT was further assessed by N_2-sorption analysis. Figure 2a shows typical adsorption-desorption isotherms for samples with both micro- and mesopores. The Brunauer–Emmett–Teller (BET) surface area and pore volume were 185 $m^2 g^{-1}$ and 0.35 $cm^3 g^{-1}$, respectively, with a pore size distribution mainly centered at 3.7 nm (Fig-

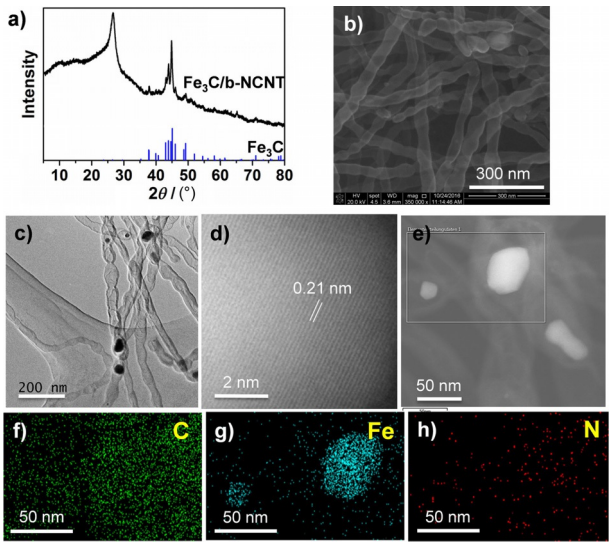

Figure 1. a) PXRD pattern. b) SEM image and c) TEM image of Fe_3C/b-NCNT. d) High-resolution HAADF-STEM image of a single Fe_3C nanoparticle in Fe_3C/b-NCNT. e) HAADF-STEM image and f–h) EDS elemental mappings of Fe_3C/b-NCNT.

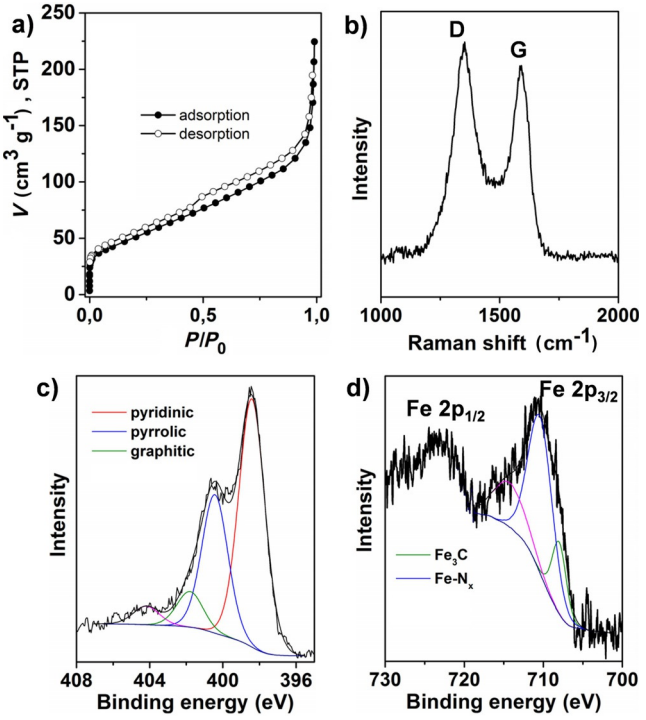

Figure 2. a) N_2 sorption isotherms. b) Raman spectrum. c) N 1s XPS spectrum and d) Fe 2p XPS spectrum for Fe_3C/b-NCNT.

ure S4). The elemental composition and graphitic nature of Fe_3C/b-NCNT were evaluated by ICP-MS analysis and Raman spectroscopy, respectively. The amount of Fe and N in Fe_3C/b-NCNT was 7.1 and 8.6 wt%, respectively. The D (1360 cm^{-1}) and G (1590 cm^{-1}) bands in the Raman spectrum provide information about the defect density and crystallinity of the sp^2 carbon. Fe_3C/b-NCNT showed an I_D/I_G value of 1.09, indicating a high degree of graphitization in agreement with the PXRD results (Figure 2b). The porous and graphitic nature of Fe_3C/b-NCNT are favorable for rapid diffusion and enhanced electrical conductivity, respectively.

High-resolution X-ray photoelectron spectroscopy (XPS) measurements were conducted to elucidate the surface properties of Fe_3C/b-NCNT. The deconvoluted N 1s spectrum showed 4 peaks, assigned to pyridinic N (398.5 eV), pyrrolic N (400.4 eV), graphitic N (401.7 eV), and oxidized N (404.2 eV) (Figure 2c). The peak at a binding energy of 398.5 eV also includes some contribution from N bound to iron (N–Fe), because there is only a small difference between the binding energies of pyridinic N and N–Fe.[5a] The amount of pyridinic N was determined to be about 59%. The Fe $2p_{3/2}$ and Fe $2p_{1/2}$ signals were centered at 710.7 eV and 723.4 eV, respectively (Figure 2d). Deconvolution of the Fe $2p_{3/2}$ region suggests the presence of Fe_3C (or metallic Fe) (707.8 eV).[3b] The main peak at 710.7 eV strongly supports the EDS and elemental analysis results that suggest Fe is present as N–coordinated Fe in the Fe_3C/b-NCNT sample.[3b,13] It must be noted that the peak at 710.7 eV assigned to Fe–N_x in Fe_3C/b-NCNT shows a 0.7 eV higher binding energy compared to the standard values ($\approx$710 eV).[3b,13] This shift suggests a lower electron density on the Fe atoms, which could originate from the interaction of Fe–N_x and Fe_3C nanoparticles.[3b] Recent reports have demonstrated that a high proportion of pyridinic N can increase the spin density and the density of π-states of the carbon atoms near the Fermi level, thus enhancing O_2 reduction.[14] Therefore, a high amount of pyridinic N together with highly dispersed Fe–N_x active sites in Fe_3C/b-NCNT is expected to enhance the intrinsic ORR activity.

The structure of Fe_3C/b-NCNT can therefore be described as crystalline Fe_3C nanoparticles that are entirely encapsulated in highly graphitic N and Fe–N_x-doped porous bamboo-like carbon nanotubes. Previous studies showed that despite the fact that the encapsulated Fe_3C nanoparticles are shielded from direct contact with electrolytes, they are able to activate surrounding graphitic carbon for the ORR,[5c,9] most likely through electronic interaction. Therefore, the unique confinement of Fe_3C nanoparticles within graphitic porous b-NCNTs is believed to efficiently improve ORR electrocatalysis. Additionally, synergistic interaction between the two species Fe–N_x and Fe_3C can further enhance ORR activity. To the best of our knowledge, this is a rare report of homogeneous bamboo-like CNTs based on a MOF as a precursor.

A possible mechanism of the formation of Fe_3C/b-NCNT is suggested in Figure 3. The final carbonization temperature required to form hollow b-NCNTs is critical. At 600 °C, the ZIF-8 structure collapses to generate carbon only. At 700 °C, a one-dimensional carbon structure is formed. TEM images confirm

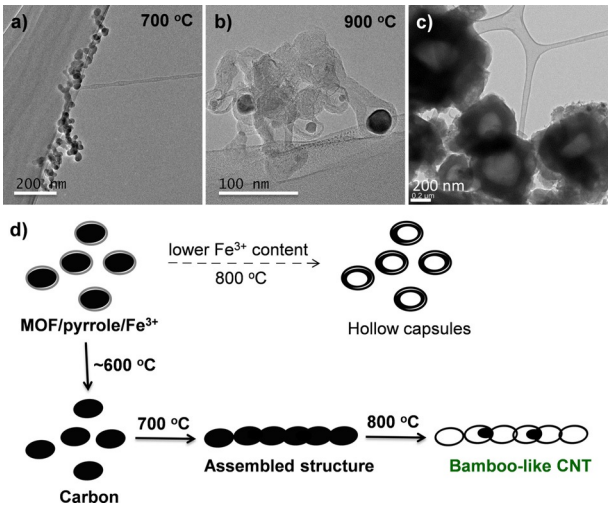

Figure 3. TEM images of samples synthesized a) at 800 °C; b) at 900 °C; and c) at 800 °C using a lower Fe^{3+} content. d) Schematic representation of Fe_3C/b-NCNT formation.

that the assembled carbon structure was not hollow in nature, and carbon particles were mostly connected in a one-dimensional chain (Figure 3a). Increasing the temperature to 800 °C led to homogeneous Fe_3C/b-NCNT (Figure 1b), whereas a higher carbonization temperature (900 °C) only produced collapsed Fe_3C/b-NCNT nanostructures (Figure 3b). The sample prepared without using ZIF-8 did not produce any CNTs (Figure S5). The mechanism of formation of the porous hollow b-NCNTs at 800 °C was further investigated by adjusting the iron content, because iron is known to catalyze CNT formation.[15] As shown in Figure 3c, hollow carbon capsules were generated at 800 °C when a lower amount of Fe^{3+} was used (2 mL of 0.1 M $FeCl_3{\cdot}6H_2O$). These findings suggest that the composite of polypyrrole with ZIF-8 synergistically produced the hollow structure at 800 °C, and required a sufficient amount of iron to catalyze homogeneous growth of the b-NCNTs. A similar coupling and conversion of hollow structures into b-NCNTs has been observed recently.[5b] Therefore, we conclude that the pyrolysis protocol, the polypyrrole/ZIF-8 composite, an effective release (vaporization) of the zinc byproduct, and the adjusted iron content are altogether responsible for the formation of the novel Fe_3C/b-NCNT catalyst.

The ORR activity of Fe_3C/b-NCNT was assessed in both alkaline and acidic electrolytes using rotating-disk-electrode (RDE) and rotating-ring-disk-electrode (RRDE) techniques. To perform these tests, 0.42 mg cm^{-2} of Fe_3C/b-NCNT was loaded onto the surface of a glassy carbon electrode. As shown in Figure 4a, Fe_3C/b-NCNT displayed an impressive ORR activity in 0.1 M KOH, with a 0.96 V onset potential, and 0.83 V at a current density of -3 mA cm^{-2}. This performance is very close to that of a commercially available state-of-art 20% Pt/C catalyst (Pt-ETEK), which produced a potential of 0.86 V at a current density of -3 mA cm^{-2}. These data are comparable to the previous activity benchmarks of Fe_3C-based ORR electrocatalysts.[3,5] Moreover, extremely low H_2O_2 oxidation currents were detected at the ring in the RRDE measurements corresponding to

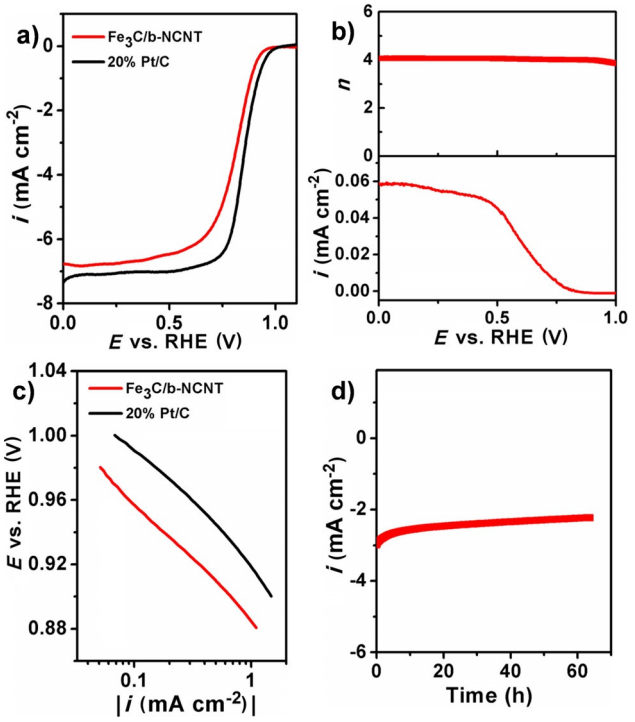

Figure 4. a) Voltammograms of Fe_3C/b-NCNT and 20 wt% Pt/C. b) Rotating ring-disk voltammogram showing the hydrogen peroxide ring current (below) and the electron transfer number (*n*; above) of Fe_3C/b-NCNT. c) Tafel plots of Fe_3C/b-NCNT and 20 wt% Pt/C. d) Chronoamperometric ORR stability measurement of Fe_3C/b-NCNT at 0.78 V vs. RHE. All measurements were obtained in O_2-saturated 0.1 M KOH solution at a rotation speed of 1600 rpm, except the chronoamperometric stability measurement, which was performed at 900 rpm. The catalyst loading was 0.42 mg cm^{-2} for Fe_3C/b-NCNT and 0.21 mg cm^{-2} (42 $\mu g_{(Pt)}$ cm^{-2}) for Pt/C. The scan rate was 5 mV s^{-1}.

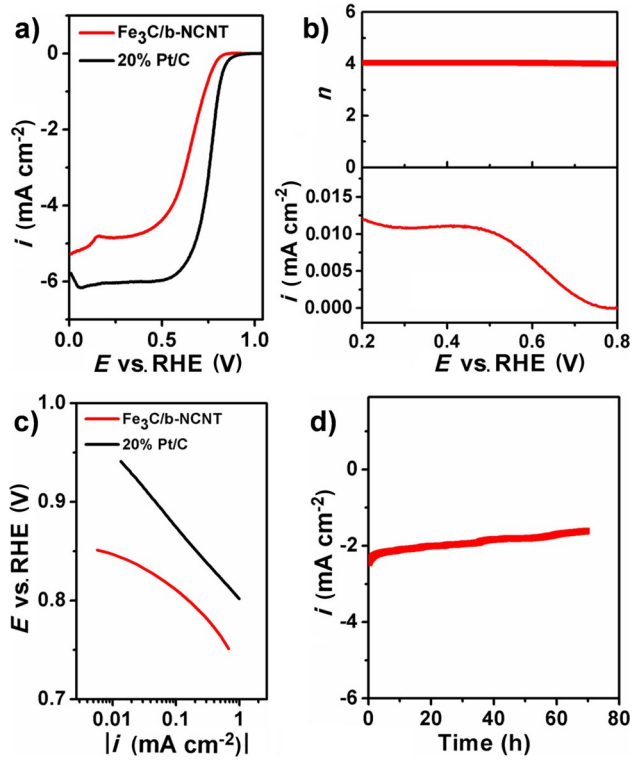

Figure 5. a) Voltammograms of Fe_3C/b-NCNT and 20 wt% Pt/C. b) Hydrogen peroxide ring current (below) and electron transfer number (*n*; above) of Fe_3C/b-NCNT. c) Tafel plots of Fe_3C/b-NCNT and 20 wt% Pt/C. d) Chronoamperometric ORR stability measurement of Fe_3C/b-NCNT at 0.61 V vs. RHE. All measurements were obtained in O_2-saturated 0.5 M H_2SO_4 solution at a rotation speed of 1600 rpm, except the chronoamperometric stability measurement which was performed at 900 rpm. The catalyst loading was 0.42 mg cm^{-2} for Fe_3C/b-NCNT and 0.21 mg cm^{-2} (42 $\mu g_{(Pt)}$ cm^{-2}) for Pt/C. The scan rate was 5 mV s^{-1}.

less than 1% H_2O_2 yield at all potentials (Figure 4b), which is much lower compared to previously reported benchmark Fe_3C-based NPMC.[5b] The number of electrons transferred per O_2 molecule (n) during the ORR was calculated to be close to 4, suggesting a predominantly four electron oxygen-reduction pathway, producing water as the main product (Figure 4b). Tafel plots of the kinetic currents, corrected for the background and mass transport effects, yielded a Tafel slope of 71.2 mV decade^{-1} for F_3C/b-NCNT at low overpotentials, close to 62.9 mV decade^{-1} for 20% Pt/C catalyst (Figure 4c). These Tafel slopes do not vary significantly from low to high overpotentials, suggesting that the mechanism of oxygen reduction with Fe_3C/b-NCNT in 0.1 M KOH follows a similar mechanism as to that with Pt/C. Therefore, corresponding to the known ORR processes on Pt/C, the transfer of the first electron is most probably the rate-determining step of the ORR on Fe_3C/b-NCNT.[5c] Chronoamperometric stability evaluation (at 0.78 V vs. a reversible hydrogen electrode, RHE) showed no significant loss in ORR activity after ≈70 hours of continuous measurement, indicating that Fe_3C/b-NCNT is able to sustain a stable ORR performance over a long period of time (Figure 4d).

Furthermore, we evaluated the ORR performance of Fe_3C/b-NCNT in 0.5 M H_2SO_4 (Figure 5). The ORR polarization curve of Fe_3C/b-NCNT exhibited a potential of 0.63 V at a current density of −3 mA cm^{-2}. In contrast, the potential at −3 mA cm^{-2} obtained with 20% Pt/C was 0.75 V (Figure 5a). The H_2O_2 yield during ORR on Fe_3C/b-NCNT in 0.5 M H_2SO_4 was below 1% over the entire investigated potential range (Figure 5b), which is lower than in 0.1 M KOH. The very low H_2O_2 yield indicates that this catalyst reduces O_2 nearly exclusively to H_2O through the 4-electron transfer process. Kinetic currents derived from the curves in Figure 5a generated Tafel plots of Fe_3C/b-NCNT and 20% Pt/C are shown in Figure 5c. Although the hydrogen peroxide generation curves are similar in both 0.1 M KOH and 0.5 M H_2SO_4, the Tafel slope of the ORR on Fe_3C/b-NCNT in 0.5 M H_2SO_4 varied significantly, from 27 mV decade^{-1} in the lower overpotential region to 83 mV decade^{-1} at higher overpotentials. This indicates that the mechanism of the ORR on Fe_3C/b-NCNT in acidic electrolyte varied significantly with potential in this narrow potential range. Moreover, the mechanism of the ORR on Fe_3C/b-NCNT is different in both electrolytes. Chronoamperometric stability studies performed at a potential of 0.61 V vs. RHE showed minimal loss in the ORR current after ≈70 hours of continuous polarization (Figure 5d). The novel Fe_3C/b-NCNT catalyst thus exhibits promising durability even in the more challenging acidic electrolytes.

Based on the structural and compositional characterization of Fe_3C/b-NCNT, we conclude that five important aspects are

responsible for its excellent ORR activity and stability: 1) High content of N (8.6 wt%) enhances hydrophilicity, thus strengthening the electrode–electrolyte interaction. 2) High percentage of pyridinic N (59%) promotes O_2 adsorption, owing to the reduced local work function of carbon.[9c] 3) Unique bamboo-like CNTs offer a higher number of edges, thus introducing a higher number of ORR active-sites. 4) High content of N-doping in b-NCNTs as a prerequisite for the formation of active Fe–N_x sites. 5) Encapsulated metal NPs can lead to unique host–guest electronic interactions, which make the outer surface of the carbon layer more active in the ORR.[9]

In summary, we developed a novel NPMC-based ORR electrocatalyst consisting of Fe_3C nanoparticles encapsulated in porous bamboo-like N-doped CNTs, synthesized by a new MOF-templated assembly approach. The excellent electrocatalytic activity, negligible hydrogen peroxide formation, and long-term stability in both acidic and basic media render Fe_3C/b-NCNT a promising low-cost, highly efficient ORR catalyst. This work provides a new protocol to construct pure-phase Fe_3C hybrids from MOF templates, and opens new avenues for further development of active and durable ORR catalysts.

Acknowledgements

Financial support from the DFG (Deutsche Forschungsgemeinschaft) in the framework of the Cluster of Excellence RESOLV (EXC1069) is gratefully acknowledged. A.A. acknowledges the Alexander von Humboldt Stiftung for a postdoctoral fellowship. The authors thank the ICAN team at the Universität Duisburg-Essen for the electron microscopy support.

Conflict of interest

The authors declare no conflict of interest.

Keywords: heterogeneous catalysis · iron carbides · metal–organic frameworks · nanostructured materials · oxygen-reduction reaction

[1] a) M. K. Debe, *Nature* **2012**, *486*, 43; b) F. Cheng, J. Chen, *Chem. Soc. Rev.* **2012**, *41*, 2172.

[2] a) Z. W. Seh, J. Kibsgaard, C. F. Dickens, I. Chorkendorff, J. K. Nørskov, T. F. Jaramillo, *Science* **2017**, https://doi.org/10.1002/science.aad4998; b) C. Cui, L. Gan, M. Heggen, S. Rudi, P. Strasser, *Nat. Mater.* **2013**, *12*, 765.

[3] a) G. A. Ferrero, K. Preuss, A. Marinovic, A. B. Jorge, N. Mansor, D. J. L. Brett, A. B. Fuertes, M. Sevilla, M.-M. Titirici, *ACS Nano* **2016**, *10*, 5922; b) W. J. Jiang, L. Gu, L. Li, Y. Zhang, X. Zhang, L. J. Zhang, J. Q. Wang, J. S. Hu, Z. Wei, L. J. Wan, *J. Am. Chem. Soc.* **2016**, *138*, 3570; c) J. Wei, Y. Liang, Y. Hu, B. Kong, G. P. Simon, J. Zhang, S. P. Jiang, H. Wang, *Angew. Chem. Int. Ed.* **2016**, *55*, 1355; *Angew. Chem.* **2016**, *128*, 1377; d) G. Ren, X. Lu, Y. Li, Y. Zhu, L. Dai, L. Jiang, *ACS Appl. Mater. Interfaces* **2016**, *8*, 4118.

[4] a) A. Miura, C. Rosero-Navarro, Y. Masubuchi, M. Higuchi, S. Kikkawa, K. Tadanaga, *Angew. Chem. Int. Ed.* **2016**, *55*, 7963; *Angew. Chem.* **2016**, *128*, 8095; b) W. Xia, A. Mahmood, Z. Liang, R. Zou, S. Guo, *Angew. Chem. Int. Ed.* **2016**, *55*, 2650; *Angew. Chem.* **2016**, *128*, 2698; c) J. Wei, Y. Liang, Y. Hu, B. Kong, J. Zhang, Q. Gu, Y. Tong, X. Wang, S. P. Jiang, H. Wang, *Angew. Chem. Int. Ed.* **2016**, *55*, 12470; *Angew. Chem.* **2016**, *128*, 12658; d) U. I. Kramm, I. Herrmann-Geppert, J. Behrends, K. Lips, S. Fiechter, P. Bogdanoff, *J. Am. Chem. Soc.* **2016**, *138*, 635; e) J. H. Zagal, M. T. M. Koper, *Angew. Chem. Int. Ed.* **2016**, *55*, 14510; *Angew. Chem.* **2016**, *128*, 14726; f) J. Masa, W. Xia, M. Muhler, W. Schuhmann, *Angew. Chem. Int. Ed.* **2015**, *54*, 10102; *Angew. Chem.* **2015**, *127*, 10240; g) C. H. Choi, C. Baldizzone, J. P. Grote, *Angew. Chem. Int. Ed.* **2015**, *54*, 12753; *Angew. Chem.* **2015**, *127*, 12944; h) K. Elumeeva, J. Ren, M. Antonietti, T.-P. Fellinger, *ChemElectroChem* **2015**, *2*, 584; i) D. Deng, L. Yu, X. Chen, G. Wang, L. Jin, X. Pan, J. Deng, G. Sun, X. Bao, *Angew. Chem.* **2013**, *125*, 389; j) H. T. Chung, J. H. Won, P. Zelenay, *Nat. Commun.* **2013**, *4*, 1922; k) Y. Liang, Y. Li, H. Wang, J. Zhou, J. Wang, T. Regier, H. Dai, *Nat. Mater.* **2011**, *10*, 780.

[5] a) Z.-Y. Wu, X.-X. Xu, B.-C. Hu, H.-W. Liang, Y. Lin, L.-F. Chen, S.-H. Yu, *Angew. Chem. Int. Ed.* **2015**, *54*, 8179; *Angew. Chem.* **2015**, *127*, 8297; b) W. Yang, X. Liu, X. Yue, J. Jia, S. Guo, *J. Am. Chem. Soc.* **2015**, *137*, 1436; c) Y. Hu, J. O. Jensen, W. Zhang, L. N. Cleemann, W. Xing, N. J. Bjerrum, Q. Li, *Angew. Chem. Int. Ed.* **2014**, *53*, 3675; *Angew. Chem.* **2014**, *126*, 3749; d) M. Xiao, J. Zhu, L. Feng, C. Liu, W. Xing, *Adv. Mater.* **2015**, *27*, 2521.

[6] a) Y. J. Sa, D.-J. Seo, J. Woo, J. T. Lim, J. Y. Cheon, S. Y. Yang, J. M. Lee, D. Kang, T. J. Shin, H. S. Shin, H. Y. Jeong, C. S. Kim, M. G. Kim, T.-Y. Kim, S. H. Joo, *J. Am. Chem. Soc.* **2016**, *138*, 15046; b) S. Yasuda, A. Furuya, Y. Uchibori, J. Kim, K. Murakoshi, *Adv. Funct. Mater.* **2016**, *26*, 738; c) K. Strickland, E. Miner, Q. Jia, U. Tylus, N. Ramaswamy, W. Liang, M.-T. Sougrati, F. Jaouen, S. Mukerjee, *Nat. Commun.* **2015**, *6*, 7343; d) L. Lin, Q. Zhu, A.-W. Xu, *J. Am. Chem. Soc.* **2014**, *136*, 11027; e) H. W. Liang, W. Wei, Z. S. Wu, X. Feng, K. Müllen, *J. Am. Chem. Soc.* **2013**, *135*, 16002; f) K. Kamiya, K. Hashimoto, S. Nakanishi, *Chem. Commun.* **2012**, *48*, 10213.

[7] a) Y. V. Kaneti, J. Tang, R. R. Salunkhe, X. Jiang, A. Yu, K. C.-W. Wu, Y. Yamauchi, *Adv. Mater.* **2017**, https://doi.org/10.1002/adma.201604898; b) J. Tang, R. R. Salunkhe, J. Liu, N. L. Torad, M. Imura, S. Furukawa, Y. Yamauchi, *J. Am. Chem. Soc.* **2015**, *137*, 1572; c) J. Tian, A. Morozan, M. T. Sougrati, M. Lefèvre, R. Chenitz, J.-P. Dodelet, D. Jones, F. Jaouen, *Angew. Chem. Int. Ed.* **2013**, *52*, 6867; *Angew. Chem.* **2013**, *125*, 7005; d) B. Liu, H. Shioyama, T. Akita, Q. Xu, *J. Am. Chem. Soc.* **2008**, *130*, 5390.

[8] a) A. Aijaz, J. Masa, C. Rösler, W. Xia, P. Weide, A. J. R. Botz, R. A. Fischer, W. Schuhmann, M. Muhler, *Angew. Chem. Int. Ed.* **2016**, *55*, 4087; *Angew. Chem.* **2016**, *128*, 4155; b) Q. L. Zhu, W. Xia, T. Akita, R. Zou, Q. Xu, *Adv. Mater.* **2016**, *28*, 6391; c) P. Yin, T. Yao, Y. Wu, L. Zheng, Y. Lin, W. Liu, H. Ju, J. Zhu, X. Hong, Z. Deng, G. Zhou, S. Wei, Y. Li, *Angew. Chem. Int. Ed.* **2016**, *55*, 10800; *Angew. Chem.* **2016**, *128*, 10958; d) Z. Li, M. Shao, L. Zhou, R. Zhang, C. Zhang, M. Wei, D. G. Evans, X. Duan, *Adv. Mater.* **2016**, *28*, 2337; e) B. Y. Xia, Y. Yan, N. Li, H. B. Wu, X. W. Lou, X. Wang, *Nat. Energy* **2016**, *1*, 15006; f) B. Y. Guan, L. Yu, X. W. Lou, *Energy Environ. Sci.* **2016**, *9*, 3092; g) H. Yang, S. J. Bradley, A. Chan, G. I. N. Waterhouse, T. Nann, P. E. Kruger, S. G. Telfer, *J. Am. Chem. Soc.* **2016**, *138*, 11872; h) P. Zhao, X. Hua, W. Xu, W. Luo, S. Chen, G. Cheng, *Catal. Sci. Technol.* **2016**, *6*, 6365; i) P. Zhao, W. Xu, X. Hua, W. Luo, S. Chen, G. Cheng, *J. Phys. Chem. C* **2016**, *120*, 11006; j) Y. Chen, C. Wang, Z. Wu, Y. Xiong, Q. Xu, S.-H. Yu, H. Jiang, *Adv. Mater.* **2015**, *27*, 5010; k) W. Zhang, Z.-Y. Wu, H.-L. Jiang, S.-H. Yu, *J. Am. Chem. Soc.* **2014**, *136*, 14385; l) H. Zhong, J. Wang, Y. Zhang, W. Xu, W. Xing, D. Xu, Y. Zhang, X. Zhang, *Angew. Chem. Int. Ed.* **2014**, *53*, 14235; *Angew. Chem.* **2014**, *126*, 14459.

[9] a) J.-P. Dodelet, R. Chenitz, L. Yang, M. Lefèvre, *ChemCatChem* **2014**, *6*, 1866; b) F. Zhang, X. Pan, Y. Hu, L. Yu, X. Chen, P. Jiang, H. Zhang, S. Deng, J. Zhang, T. B. Bolin, S. Zhang, Y. Huang, X. Bao, *Proc. Natl. Acad. Sci. USA* **2013**, *110*, 14861; c) D. Deng, L. Yu, X. Chen, G. Wang, L. Jin, X. Pan, J. Deng, G. Sun, X. Bao, *Angew. Chem. Int. Ed.* **2013**, *52*, 371; *Angew. Chem.* **2013**, *125*, 389.

[10] C. Galeano, J. C. Meier, V. Peinecke, H. Bongard, I. Katsounaros, A. A. Topalov, A. Lu, K. J. J. Mayrhofer, F. Schüth, *J. Am. Chem. Soc.* **2012**, *134*, 20457.

[11] T. A. Wezendonk, V. P. Santos, M. A. Nasalevich, Q. S. E. Warringa, A. I. Dugulan, A. Chojecki, A. C. J. Koeken, M. Ruitenbeek, G. Meima, H. U. Islam, G. Sankar, M. Makkee, F. Kapteijn, J. Gascon, *ACS Catal.* **2016**, *6*, 3236.

[12] a) H. Zhang, T. Wang, J. Wang, T. D. Dao, M. Li, G. Liu, X. Meng, K. Chang, L. Shi, T. Nagao, J. Ye, *Adv. Mater.* **2016**, *28*, 3703; b) E. Proietti, F. Jaouen, M. Lefevre, N. Larouche, J. Tian, J. Herranz, J.-P. Dodelet, *Nat. Commun.* **2011**, *2*, 416.

[13] R. Cao, R. Thapa, H. Kim, X. Xu, M. Gyu Kim, Q. Li, N. Park, M. Liu, J. Cho, *Nat. Commun.* **2013**, *4*, 2076.

[14] a) Y. Zhao, K. Watanabe, K. Hashimoto, *J. Am. Chem. Soc.* **2012**, *134*, 19528; b) J. Liang, Y. Jiao, M. Jaroniec, S. Z. Qiao, *Angew. Chem. Int. Ed.* **2012**, *51*, 11496; *Angew. Chem.* **2012**, *124*, 11664; c) K. Gong, F. Du, Z. Xia, M. Durstock, L. Dai, *Science* **2009**, *323*, 760.

[15] a) N. Li, X. X. Chen, L. Stoica, W. Xia, J. Qian, J. Assmann, W. Schuhmann, M. Muhler, *Adv. Mater.* **2007**, *19*, 2957; b) K. Hernadi, A. Fonseca, J. B. Nagy, D. Bernaerts, A. A. Lucas, *Carbon* **1996**, *34*, 1249.

Manuscript received: March 28, 2017
Accepted manuscript online: March 29, 2017
Version of record online: May 2, 2017